Hindawi
Journal of Nanomaterials
Volume 2018, Article ID 7859747, 11 pages
https://doi.org/10.1155/2018/7859747

Research Article

Geometry-Controlled Carbon Coils by SF_6 Flow Injection Time with Reaction Temperature

Dong-Chul Kim and Sung-Hoon Kim

Department of Engineering in Energy & Applied Chemistry, Silla University, Busan 617-736, Republic of Korea

Correspondence should be addressed to Sung-Hoon Kim; shkim@silla.ac.kr

Received 18 August 2017; Revised 26 January 2018; Accepted 15 February 2018; Published 18 March 2018

Academic Editor: Zafar Iqbal

Carbon nanocoils and/or microcoils were synthesized using C_2H_2 as the source gas along with the injection of SF_6 as an incorporated additive gas under the thermal chemical vapor deposition (TCVD) system. To control the geometries of the carbon coils, we varied the SF_6 flow injection time at different reaction temperature ranges. At the lowest reaction temperature (550°C), carbon microcoils were dominantly formed within a relatively short initial SF_6 flow injection time (less than 5 min). By increasing the SF_6 flow injection time, carbon nanocoils could be well developed on the entire surface of the sample. At 750°C, the formation of carbon microcoils dominated over the entire sample surface, irrespective of the SF_6 flow injection time. Based on these results, the growth mechanism for the dominantly formed carbon coils was suggested and discussed. In addition, the causes for the dominant formation of carbon nanocoils and/or microcoils according to the SF_6 flow injection times with the different reaction temperatures were analyzed.

1. Introduction

Owing to their unique shape, carbon coils have been noticed to be superior in specific material characteristics to carbon nanotubes. Compared with the linear type geometry of carbon nanotubes, carbon coils show a helical type spring-like geometry. Therefore, they are supposed to give the promising materials characteristics such as superelasticity [1–3], good chirality [4], and high shielding effectiveness for electromagnetic wave radiation especially in high frequency regions [5–8]. Their superior material characteristics allow them to be good potential candidates for micro/nanodevices [9, 10], polymer reinforced constituents [11, 12], hydrogen storage media [13–15], chiral catalysts [16], electromagnetic wave absorbers [17], and sensors [18–23]. To extend the practical applications of carbon coils, their geometries should be controlled to enhance the electrical properties of helical coils, which might vary depending on their geometry, including the diameter, as in the case of the carbon nanotubes [24]. To date, several methods have been attempted to obtain geometry-controlled carbon coils [25–33]. Among these methods, the in situ process during the carbon coils synthesis reaction has been noticed because the in situ process can be combined with the ex situ method. Consequently, these combined methods can provide an advantage for the formation of the geometry-controlled carbon coils.

The cycling on/off modulation of the flow of source gases has recently come into focus as an in situ method for the formation of geometry-controlled carbon coils [34, 35]. These carbon coils could be obtained by adjusting the number of cycles for the on/off modulation of the flow of source gases during the reaction [36]. The manipulation of the cycling on/off time ratio of the flow of source gases during the reaction was also reported to produce geometry-controlled carbon coils [37]. A modified cycling on/off method, that is, with the different injection sequences of the flow of source gases, had been reported to be effective in controlling the carbon coils geometries [38]. In addition, several studies were carried out using C_2H_2/SF_6 gases to form the geometry-controlled carbon coils [38–41]. Despite these reports, the extension of the in situ method for geometry control of the carbon coils even to a low temperature (below 600°C) would be required to expand the application area of the carbon coils.

Table 1: Experimental conditions for the deposition of samples A–L.

Samples	C_2H_2 flow rate (sccm)	C_2H_2 flow injection time (min)	SF_6 flow rate (sccm)	SF_6 flow injection time (min)	Total pressure (Torr)	Substrate temperature (°C)
A	500	60	40	5	100	550
B	500	60	40	15	100	550
C	500	60	40	30	100	550
D	500	60	40	60	100	550
E	500	60	40	5	100	650
F	500	60	40	15	100	650
G	500	60	40	30	100	650
H	500	60	40	60	100	650
I	500	60	40	5	100	750
J	500	60	40	15	100	750
K	500	60	40	30	100	750
L	500	60	40	60	100	750

In this work, we carried out the in situ cycling on/off modulation process of the flow of source gases at a low temperature (550°C). We compared the as-grown morphologies of the carbon coils produced at a low temperature with the ones from a high temperature (750°C). The characteristics of the carbon coils according to the reaction temperature were also investigated. Based on these results, the dominant growth modes for the formation of the geometry-controlled carbon coils at a low temperature (550°C) or high temperature (750°C) were discussed and proposed.

2. Experimental Details

Alumina (Al_2O_3) plates with areas of 3.0×13.0 cm^2 and about 2 mm thickness were used as the substrate in this work. For the Ni catalyst preparation, approximately 0.1 g of bunch-type Ni powder (99.7%) with particle diameters ranging from 100 to 200 μm was spread onto the substrate. Thermal chemical vapor deposition (TCVD) system was employed with C_2H_2 as the source gas and SF_6 as the additive gas for the formation of the carbon coils. The total pressure in the reactor was maintained at 100 Torr. The flow rates for C_2H_2 and SF_6 were fixed at 500 and 40 standard cm^3 per minute (sccm), respectively. The injection time of C_2H_2 was fixed at 60 min. According to the different reaction processes, the SF_6 flow injection time was varied with the different reaction temperatures. Twelve samples prepared with different SF_6 flow injection times with different reaction temperatures were intensively studied. The reaction conditions of the twelve samples for this work are shown in Table 1.

Detailed morphologies and chemical compositions of the samples were examined using a field emission scanning electron microscope (FESEM, Hitachi S-4200). The crystalline phases were identified through X-ray diffraction (XRD, Shimadzu 6000) using Cu Kα radiation (λ = 0.1541 nm) in the angular range of $10^\circ < 2\theta < 60^\circ$. The quality of the carbon coils was investigated using a micro-Raman spectrometer (Renishaw inVia Reflex) with an Ar-ion laser (wavelength λ = 514.5 nm) in the spectral range of 1,000–2,000 cm^{-1}.

3. Results and Discussion

At 550°C, four samples were prepared with SF_6 flow injection times of 5 min (sample A), 15 min (sample B), 30 min (sample C), and 60 min (sample D). Figure 1 shows FESEM images of the surface morphologies of samples A–D.

In the case of SF_6 flow injection time of 5 min (the shortest SF_6 flow injection time in this work), we observed the formation of coil morphology on the whole surface of sample A as shown in Figure 1(a). The inset of Figure 1(a) shows the magnified image of the area enclosed in the dashed square in Figure 1(a): the coexistence of well-developed carbon microcoils with untangled carbon microcoils is visible. So, this morphology was understood to be formed by a lot of the double-helix carbon microcoils. When the SF_6 flow injection time was increased from 5 to 15 min, various kinds of carbon coil-like geometries could be observed on the surface of sample B as shown in Figure 1(b). In this case, the single-helix carbon nanocoils occasionally appeared as shown in the magnified image (inset of Figure 1(b)) of the region enclosed in the dashed square in Figure 1(b). A further increase in the SF_6 flow injection time to 30 min gave rise to an increase in the density of the single-helix carbon nanocoils with linear carbon nanofilaments on sample C (see Figure 1(c)). Indeed, the continuous injection of SF_6 flow during the whole reaction time (60 min) resulted in the dominant formation of single-helix carbon nanocoils with linear carbon nanofilaments over the whole surface of sample D (see Figure 1(d)).

The results as shown in Figure 1 reveal that the double-helix carbon microcoils were exclusively formed by the relatively short injection time (5 min) of the SF_6 flow. On the other hand, the single-helix carbon nanocoils could be dominantly formed on the whole surface of the sample by the continuous injection of SF_6 during the whole reaction time (60 min).

We carried out the same experiment at 650°C and observed a similar tendency of geometry change according to the SF_6 flow injection time, as shown in Figure 2. In this

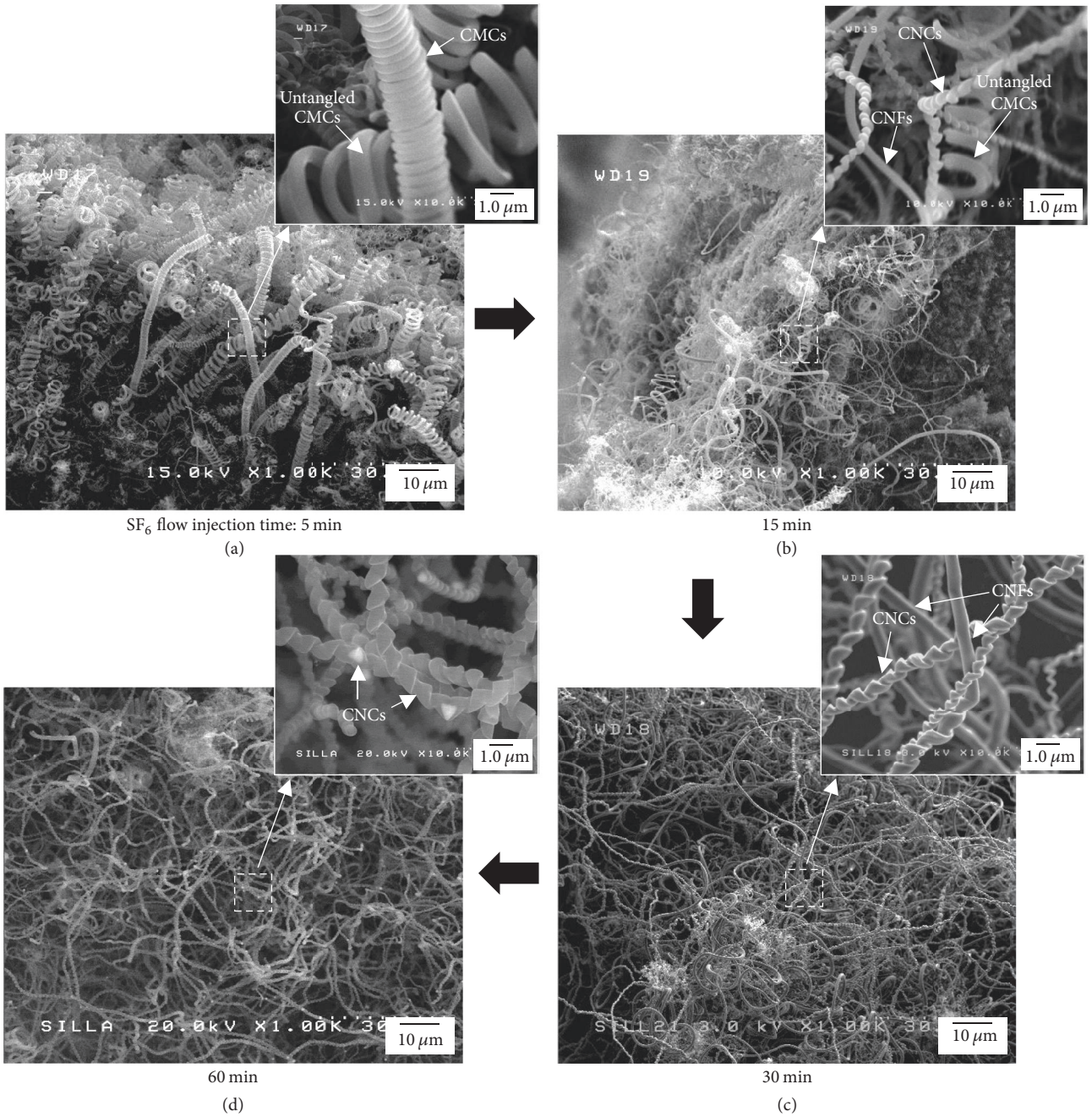

Figure 1: FESEM images of (a) sample A, (b) sample B, (c) sample C, and (d) sample D. The insets of (a)–(d) show the magnified images for the dashed square areas in (a)–(d). CMCs, CNCs, and CNFs in the insets mean the carbon microcoils, the carbon nanocoils, and the carbon nanofilaments, respectively.

case, however, the extent of geometry control by the SF_6 flow injection time deteriorated slightly. The formation of carbon nanocoils alone could not be obtained by the continuous SF_6 flow injection during the whole reaction time (60 min). Instead, linear carbon nanofilaments with carbon nanocoils were observed on the surface of sample H (see Figure 2(d)).

The results in Figures 1 and 2 confirm that the carbon microcoils could be exclusively obtained by the shortest injection time (5 min) of SF_6 flow, whereas the dominant formation of the carbon nanocoils was achieved by the continuous SF_6 flow injection (60 min) at 550°C. In other words, the geometries of the carbon coils can be controlled simply by the manipulation of SF_6 flow injection times at 550°C.

The causes for these results are understood as follows. After the carbon coils formation reaction, the following was calculated: product/catalyst mass ratio, that is, the ratio of the amount of the carbon coils-related product to the amount of the used catalyst. As shown in Figure 3 and Table 2, the ratio for sample A (SF_6 flow injection time = 5 min) was

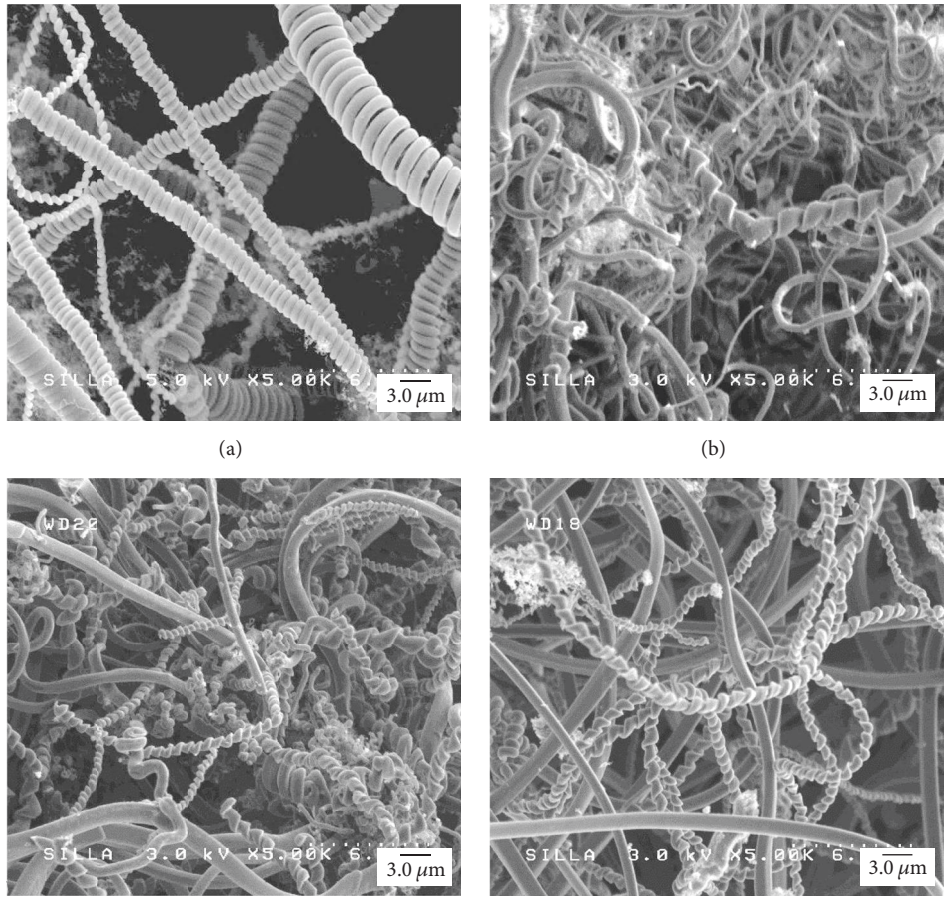

Figure 2: FESEM images of (a) sample E, (b) sample F, (c) sample G, and (d) sample H. Having the corresponding experimental parameters, except the reaction temperature, of samples A–D at 650°C.

Table 2: The amount of the carbon coils-related product to the amount of the used catalyst, according to the samples.

Samples	Product (g)	Used catalyst (g)	Product/catalyst (ratio)	Substrate temperature (°C)
A	15.79	0.10	157.90	550
B	15.86	0.11	144.18	550
C	9.60	0.11	87.27	550
D	5.62	0.10	56.20	550
I	6.67	0.12	55.58	750
J	5.23	0.10	52.30	750
K	3.32	0.11	30.18	750
L	2.98	0.10	29.80	750

157.90, more than double the 56.20 for sample D (SF_6 flow injection time = 60 min). This result indicates that the carbon nanostructures related to the carbon coils were effectively etched away with increments in the SF_6 flow injection time.

In previous reports, the double-helix-type carbon microcoils were known to be formed from the various-shaped carbon nanostructures, namely, single-helix carbon nanocoils, wave-like carbon nanofilaments, and linear carbon nanofilaments [42, 43]. We could also observe the formation of the carbon microcoils from wave-like carbon nanofilaments (Figure 4(a)), from the carbon nanocoils (Figure 4(b)), and from untangled carbon microcoils (Figure 4(c)). At 550°C, the formation of the carbon microcoils was frequently observed from the carbon nanocoils (see Figure 4(b)).

In any case, the developed carbon microcoils are located in the upper region of the as-growing carbon coils. Because of their location, they may be the first to encounter the incoming fluorine element from the SF_6 flow. Consequently, they would readily be etched away by the fluorine due to fluorine's intrinsic characteristics to etch other materials.

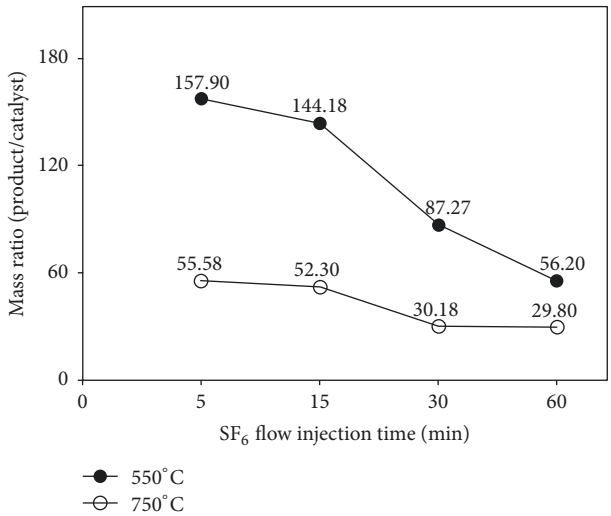

Figure 3: The product/catalyst mass ratio, namely, the ratio of the amount of the carbon coils-related product to the amount of the used catalyst, according to the samples.

Therefore, the increase in the SF_6 flow injection time led to the decrease in the number of the as-grown carbon microcoils. In addition, the crystallinity of the carbon coils was higher than those of various types of carbon nanofilaments [44]. Therefore, the carbon nanocoils, located in the lower part of the as-growing carbon coils, would be dominantly formed under the condition of continuous SF_6 flow injection. This way, the dominant formation of the carbon microcoils and nanocoils could be achieved by the manipulation of the SF_6 flow injection time at 550°C.

Figure 5 shows the mechanism, called the preferential etching and survival mechanism, for the formation of geometry-controlled carbon coils by the manipulation of SF_6 flow injection times at the lowest reaction temperature (550°C) in this work.

The preferential etching and survival mechanism is proposed to be as follows:

(1) The carbon microcoils were usually formed from the carbon nanofilaments and/or the carbon nanocoils. The developed carbon microcoils were mainly located in the upper position of the as-growing carbon coils.

(2) The developed carbon microcoils were preferentially etched away by the incoming fluorine-related elements due to their location on the upper position of the as-growing carbon coils.

(3) Owing to the higher crystallinities of the carbon coils than those of the various types of carbon nanofilaments, the carbon nanocoils would survive in the case of continuous SF_6 flow injection.

At 750°C, we could obtain different geometry change of the carbon coils according to the SF_6 flow injection time. As shown in Table 1, four samples were prepared according to the SF_6 flow injection times of 5 min (sample I), 15 min (sample J), 30 min (sample K), and 60 min (sample L) at 750°C. Figure 6 shows FESEM images of the surface morphologies of samples I–L. In the case of SF_6 flow injection time of 5 min, we could see many linear structures on the surface of sample I as shown in Figure 6(a). The magnified image indicates the well-developed individual carbon microcoil for the line shape (see the inset in Figure 6(a)). The lengths of the individual carbon microcoils seemed to be much longer than those at 650°C or 550°C (compare Figure 6(a) with Figures 1(a) and 2(a)). Furthermore, most of the individual carbon microcoils on sample I had a well-developed shape, compared with those of the samples at 650°C or 550°C (compare Figure 6(a) with Figures 1(a) and 2(a)). These results reveal that the development of the individual carbon microcoil can be enhanced by increasing the reaction temperature from 550°C to 750°C.

In addition, the amount of the product/catalyst mass ratios for the samples at 750°C is much lower than those at 550°C (see Figure 3 and Table 2). This result strongly indicates that the etching effectiveness for the carbon nanostructures related to the carbon coils by fluorine's intrinsic characteristics would increase with increasing reaction temperature from 550°C to 750°C. The product/catalyst mass ratio for sample I (the SF_6 flow injection time = 5 min) was 55.58, less than double the 29.80 for sample L (the SF_6 flow injection time = 60 min). This result also reveals that the etching effectiveness of the carbon nanostructures related to the carbon coils was not significantly improved with increasing SF_6 flow injection time at 750°C, unlike in the case of 550°C.

With increasing SF_6 flow injection times from 5 to 30 min, the double-helix carbon microcoils seemed to deteriorate as shown in Figure 6. In the case of the continuous injection of the SF_6 flow during the whole reaction time (60 min), untangled carbon microcoils were mostly seen on the entire surface of sample L (see Figure 6(d)). The results in Figure 6 indicate that the well-developed carbon microcoils were formed at a relatively short injection time (5 min) of SF_6 flow. When the SF_6 flow injection time was increased from 5 to 30 min, the carbon microcoils were still present on the surface of the samples. However, the geometries of the carbon microcoils seemed to have deteriorated. Finally, untangled coils were realized by the continuous SF_6 flow injection during the whole reaction time (60 min).

The results in Figure 6 confirm that the carbon microcoils were predominantly formed over the whole surface of the sample at 750°C, irrespective of the SF_6 flow injection time. Indeed, the carbon microcoils seemed to be untangled by the continuous SF_6 flow injection. The cause for this result is understood as follows. After carbon coils formation reaction, the mass ratio of the amount of the product to the amount of the used catalyst was also calculated as shown in Figure 3 and Table 2. This ratio for sample I (the SF_6 flow injection time = 5 min, at 750°C) was 55.58, around one-third of that for sample A (the SF_6 flow injection time = 5 min, at 550°C). In addition, the mass ratio for sample L is slightly lower than that for sample I. These results indicate that the etching aspect of the carbon nanostructures was more effectively influenced by the reaction temperature rather than the injection time of the SF_6 flow.

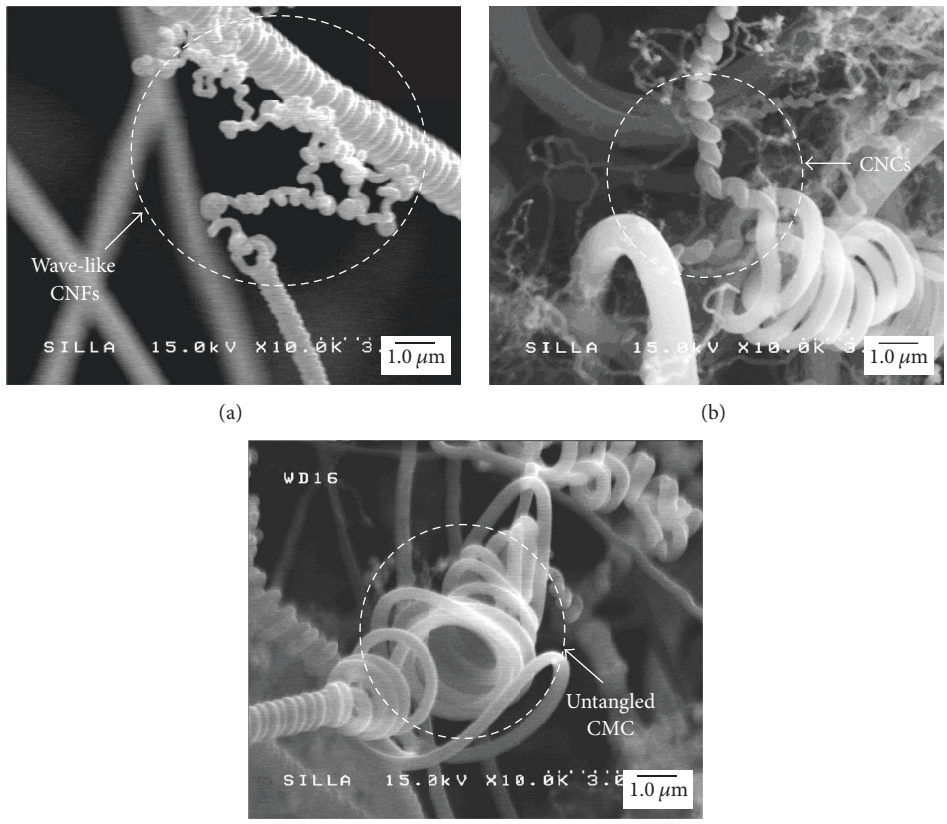

FIGURE 4: FESEM images showing the formation of the carbon microcoils (a) from the wave-like carbon nanofilaments in sample I, (b) from the carbon nanocoils in sample A, and (c) from the untangled carbon microcoils in sample I.

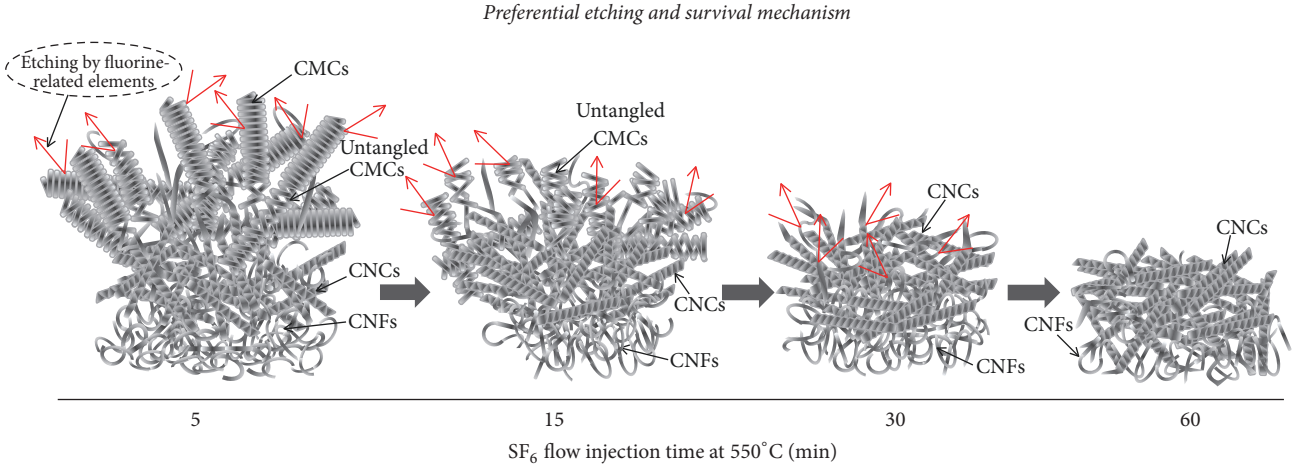

CMCs: carbon microcoils
CNCs: carbon nanocoils
CNFs: carbon nanofilaments

FIGURE 5: The schematic diagram for the preferential etching and survival mechanism to form the geometry-controlled carbon coils at the lowest reaction temperature (550°C) in this work.

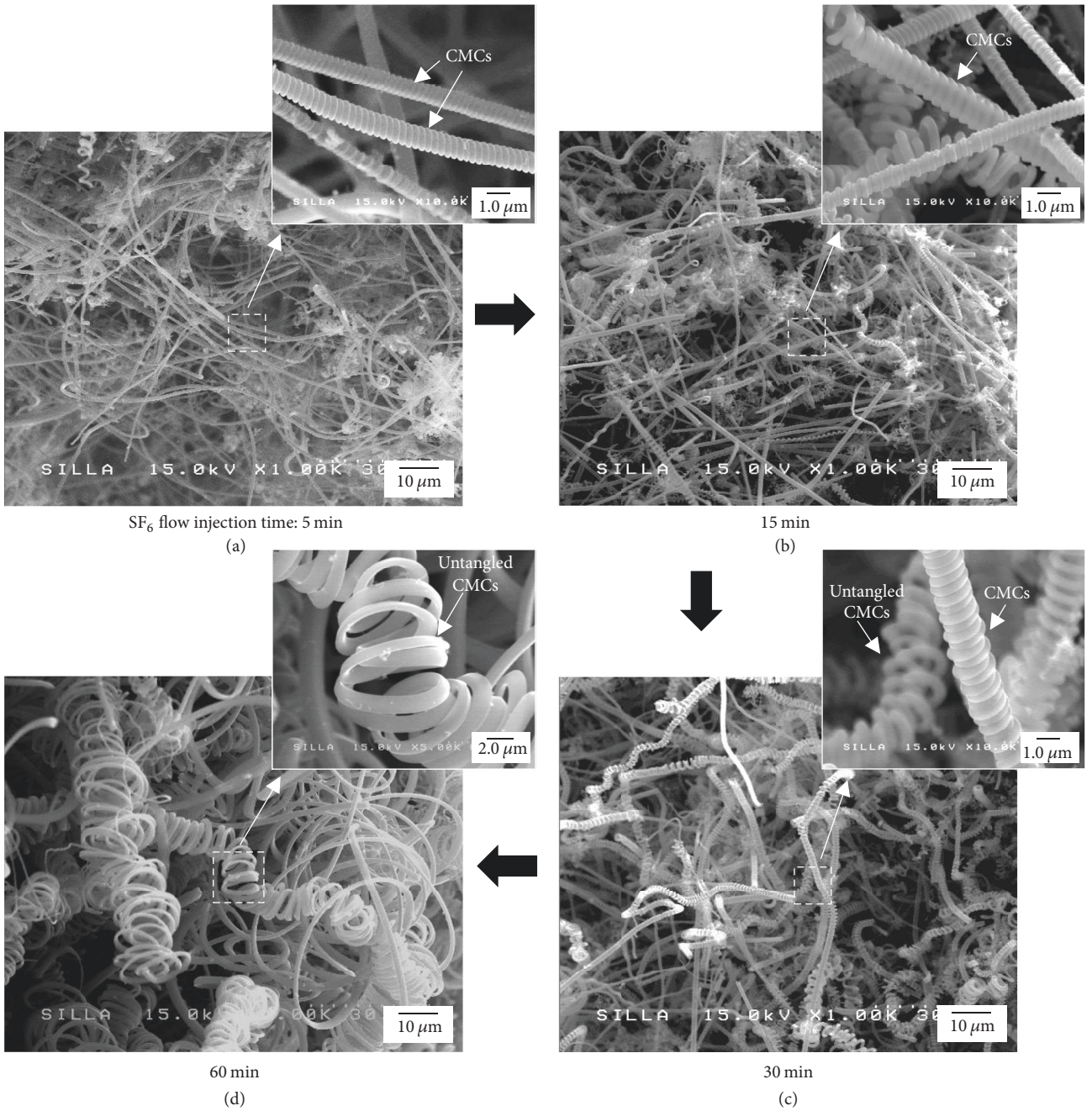

Figure 6: FESEM images of (a) sample I, (b) sample J, (c) sample K, and (d) sample L. The insets of (a)–(d) show the magnified images for the dashed square areas in (a)–(d).

At 750°C, we observed the formation of the carbon microcoils from the untangled carbon microcoils rather than the carbon nanocoils as shown in Figure 4(c). Therefore, we propose the mechanism, called the survival mechanism, for the formation of the geometry-controlled carbon microcoils by the manipulation of SF_6 flow injection times at the high reaction temperature (750°C) as shown in Figure 7.

The survival mechanism is proposed to be as follows:

(1) The carbon microcoils were usually formed from the carbon nanofilaments and/or the untangled carbon microcoils. Owing to the high reaction temperature, the carbon microcoils were readily formed and rapidly grown.

(2) The high reaction temperature enhanced the etching rate of the carbon nanostructures. Consequently, the amount of the as-grown carbon nanostructures is dramatically decreased even under the short SF_6 flow injection time. With increasing SF_6 flow injection time, the amount of the as-grown carbon nanostructures slightly decreased compared with that at the low reaction temperature.

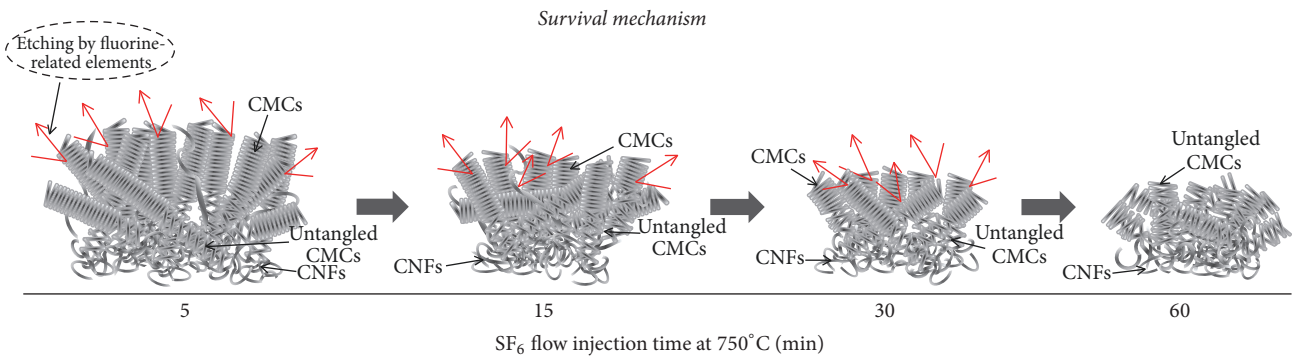

CMCs: carbon microcoils
CNFs: carbon nanofilaments

FIGURE 7: The schematic diagram for the survival mechanism to form the geometry-controlled carbon coils at the highest reaction temperature (750°C) in this work.

(3) Owing to the high crystallinities of the carbon microcoils being higher than that of any other carbon nanostructure, the double-helix carbon microcoils survived even under the condition of continuous SF_6 flow injection.

The crystallinity and crystal structures of samples A, D, I, and L were investigated by XRD using the Scherrer equation. Figure 8 shows two remarkable peaks around 24.0° and 43.0° assigned to the typical graphitic (002) and (100)/(101) planes, respectively [44].

Table 3 shows the intensities and the 2θ values of the (002) positions for the different samples. Comparing the (002) peaks of the different samples, it is noticed that the intensities and the 2θ value of sample A are higher than those of sample D. Consequently, the (002) peaks of the carbon microcoils have a higher intensity than those of the carbon nanocoils. In addition, sample A has a lower full width at half maximum (FWHM) than sample D, indicating a reduced line broadening.

Using the Scherrer equation, $L_c = 0.91\lambda/(\beta \cos\theta)$ [45–47], the XRD data (the peak intensities and the 2θ values of the maximum positions of the (002) plane) allow for the calculation of the average nanocrystalline sizes along the c-direction (L_c), listed in Table 3. The L_c value of sample A is higher than that of sample D.

Based on the results of the XRD data, we can confirm that the samples with the predominant carbon microcoils formation (sample A) have a more regular crystal structure compared with the sample with the predominant carbon nanocoils formation (sample D). This result strongly confirms that the shortest SF_6 flow injection time gives rise to the most regular crystal structure of the carbon coils at 550°C. At 750°C, similarly, sample I having the shortest SF_6 flow injection time in this work had the most regular crystal structure of the carbon microcoils as shown in Figure 8 and Table 3.

Meanwhile, the quality of the carbon coils of the different samples was also investigated by micro-Raman spectroscopy as shown in Figure 9. The D and G peaks of all samples

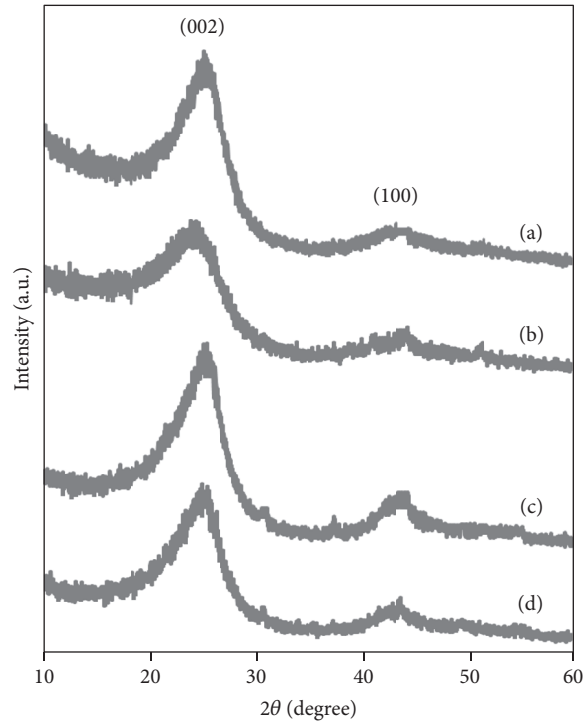

FIGURE 8: XRD spectra of (a) sample A, (b) sample D, (c) sample I, and (d) sample L.

were observed around 1,350 cm^{-1} and 1,600 cm^{-1}, respectively [48, 49]. From the curve fitting (see the inset of Figure 9) of the Raman spectra, the corresponding I_D/I_G values were calculated [49, 50]. Table 4 shows the I_D/I_G values and the peak top positions of the G and D bands of the different samples. The G and D bands are known to be associated with the stretching vibrations of graphite and the disordered states of sp^2-hybridized carbon, respectively [51, 52].

As shown in Table 4, the I_D/I_G value of sample I was lower than those of the other samples, indicating the larger

Table 3: Intensities, 2θ values, FWHM, and average size of the nanocrystals along the c-direction (L_c) obtained from the XRD (002) reflections of the samples.

Samples	2θ values of the peaks at (002) plane (degree)	Peak intensities of (002) plane (arbitrary unit)	FWHM of the peak at (002) plane (β, radian)	The average nanocrystal sizes (L_c), $L_c = 0.91\lambda/\beta\cos\theta$ (nm)
A	25.38	980	0.0502	2.81
D	24.10	560	0.0634	2.26
I	25.70	986	0.0481	3.03
L	25.20	604	0.0572	2.47

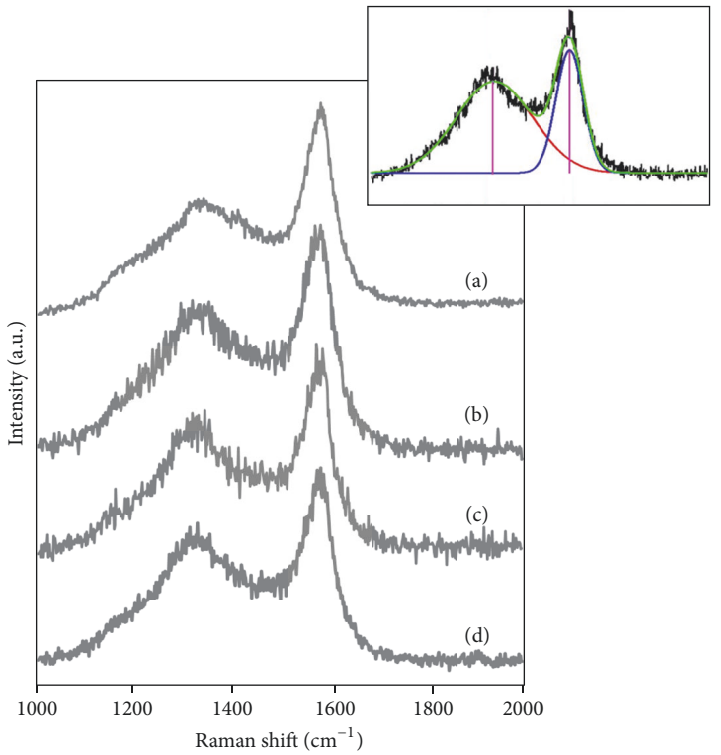

Figure 9: Micro-Raman spectra of (a) sample A, (b) sample D, (c) sample I, and (d) sample L. The inset shows the curve fitting of the spectrum of sample A.

percentage of the ordered carbon phase. Samples A and I are dominated by carbon microcoils and have lower I_D/I_G value compared with those of samples D and L. In addition, the peak top position of the G band shifted downward for samples A and I. On the other hand, the D band shifted strongly upward for samples A and I. These tendencies also indicate the more pronounced polycrystalline structure for the carbon coils of samples A and I. Based on these results presented in Figures 8 and 9 and Tables 3 and 4, we confirm that the shortest SF_6 flow injection time can promote the dominant formation of the carbon microcoils having a regularly developed crystal structure regardless of the reaction temperature.

4. Conclusion

At the low reaction temperature (550°C), carbon microcoils were exclusively obtained by the shortest SF_6 flow injection time (5 min), whereas the dominant formation of the carbon nanocoils was achieved by the continuous SF_6 flow injection. At the high reaction temperature (750°C), the dominant formation of the well-developed carbon microcoils over the whole surface of the sample was observed, irrespective of the SF_6 flow injection time. We suggest the preferential etching and survival mechanism at 550°C and, on the other hand, the survival mechanism at 750°C for the growth modes of the formation of the carbon nano- or microcoils according to the SF_6 flow injection time. The cause for the formation of the different geometries of the carbon coils according to the SF_6 flow injection time with the different reaction temperatures was discussed in detail.

Conflicts of Interest

The authors declare that they have no conflicts of interest.

Table 4: The peak top positions of G and D bands of the Raman spectra and the ratios I_D/I_G calculated from the fitted Raman spectra.

Samples	G-band peak-top (cm^{-1})	D-band peak-top (cm^{-1})	I_D/I_G
A	1596.93	1354.77	0.58
D	1598.43	1331.70	0.67
I	1590.97	1357.84	0.56
L	1598.43	1343.47	0.64

Acknowledgments

This research was supported by the Basic Science Research Program through the National Research Foundation of Korea (NRF) funded by the Ministry of Education (NRF-2017R1D1A3B03035901).

References

[1] S. Motojima, X. Chen, S. Yang, and M. Hasegawa, "Properties and potential applications of carbon microcoils/nanocoils," *Diamond and Related Materials*, vol. 13, no. 11-12, pp. 1989–1992, 2004.

[2] X. Chen, S. Motojima, and H. Iwanga, "Vapor phase preparation of super-elastic carbon micro-coils," *Journal of Crystal Growth*, vol. 237-239, no. 1-4, article 2174, pp. 1931–1936, 2002.

[3] A. Volodin, M. Ahlskog, E. Seynaeve, C. Van Haesendonck, A. Fonseca, and J. B. Nagy, "Imaging the elastic properties of coiled carbon nanotubes with atomic force microscopy," *Physical Review Letters*, vol. 84, no. 15, pp. 3342–3345, 2000.

[4] H. Wang, S. Yang, and X. Chen, "Progress study of micro carbon coils," *IOP Conference Series: Materials Science and Engineering*, vol. 274, p. 012108, 2017.

[5] X. Jian, X. Chen, Z. Zhou et al., "Remarkable improvement in microwave absorption by cloaking a micro-scaled tetrapod hollow with helical carbon nanofibers," *Physical Chemistry Chemical Physics*, vol. 17, no. 5, pp. 3024–3031, 2015.

[6] S. Motojima, Y. Noda, S. Hoshiya, and Y. Hishikawa, "Electromagnetic wave absorption property of carbon microcoils in 12-110 GHz region," *Journal of Applied Physics*, vol. 94, no. 4, pp. 2325–2330, 2003.

[7] N. Tang, W. Zhong, C. Au et al., "Synthesis, microwave electromagnetic, and microwave absorption properties of twin carbon nanocoils," *The Journal of Physical Chemistry C*, vol. 112, pp. 19316–19323, 2008.

[8] L. Liu, P. He, K. Zhou, and T. Chen, "Microwave absorption properties of carbon fibers with carbon coils of different morphologies (double microcoils and single nanocoils) grown on them," *Journal of Materials Science*, vol. 49, no. 12, pp. 4379–4386, 2014.

[9] N. Tang, W. Kuo, C. Jeng, L. Wang, K. Lin, and Y. Du, "Coil-in-coil carbon nanocoils: 11 gram-scale synthesis, single nanocoil electrical properties, and electrical contact improvement," *ACS Nano*, vol. 4, no. 2, pp. 781–788, 2010.

[10] H.-S. Chiu, P.-I. Lin, H.-C. Wu, W.-H. Hsieh, C.-D. Chen, and Y.-T. Chen, "Electron hopping conduction in highly disordered carbon coils," *Carbon*, vol. 47, no. 7, pp. 1761–1769, 2009.

[11] K. Yoshimura, K. Nakano, T. Miyake, Y. Hishikawa, and S. Motojima, "Effectiveness of carbon microcoils as a reinforcing material for a polymer matrix," *Carbon*, vol. 44, no. 13, pp. 2833–2838, 2006.

[12] T. Katsuno, X. Chen, S. Yang et al., "Observation and analysis of percolation behavior in carbon microcoils/silicone-rubber composite sheets," *Applied Physics Letters*, vol. 88, no. 23, Article ID 232115, 2006.

[13] A. L. M. Reddy, R. I. Jafri, N. Jha, S. Ramaprabhu, and P. M. Ajayan, "Carbon nanocoils for multi-functional energy applications," *Journal of Materials Chemistry*, vol. 21, no. 40, pp. 16103–16107, 2011.

[14] Y. Furuya, T. Hashishin, H. Iwanaga, S. Motojima, and Y. Hishikawa, "Interaction of hydrogen with carbon coils at low temperature," *Carbon*, vol. 42, no. 2, pp. 331–335, 2004.

[15] S. V. Jaybhaye, M. Sharon, M. Sharon, and L. N. Singh, "Study of hydrogen adsorption by spiral carbon nano fibers synthesized from acetylene," *Synthesis and Reactivity in Inorganic, Metal-Organic, and Nano-Metal Chemistry*, vol. 36, no. 1, pp. 37–42, 2006.

[16] S. Motojima and X. Chen, "Preparation and characterization of carbon microcoils (CMCs)," *Bulletin of the Chemical Society of Japan*, vol. 80, no. 3, pp. 449–455, 2007.

[17] G.-H. Kang and S.-H. Kim, "Effect of incorporating carbon nanocoils on the efficiency of electromagnetic-wave shielding of carbon-nanomaterial composites," *Applied Surface Science*, vol. 380, pp. 114–118, 2016.

[18] Y. Kato, N. Adachi, T. Okuda, T. Yoshida, S. Motojima, and T. Tsuda, "Evaluation of induced electromotive force of a carbon micro coil," *Japanese Journal of Applied Physics*, vol. 42, no. 8, pp. 5035–5037, 2003.

[19] A. Volodin, D. Buntinx, M. Ahlskog, A. Fonseca, J. B. Nagy, and C. Van Haesendonck, "Coiled carbon nanotubes as self-sensing mechanical resonators," *Nano Letters*, vol. 4, no. 9, pp. 1775–1779, 2004.

[20] X. Chen, S. Yang, M. Hasegawa, K. Kawabe, and S. Motojima, "Tactile microsensor elements prepared from arrayed superelastic carbon microcoils," *Applied Physics Letters*, vol. 87, no. 5, Article ID 054101, 2005.

[21] S. Yang, X. Chen, and S. Motojima, "Tactile sensing properties of protein-like single-helix carbon microcoils," *Carbon*, vol. 44, no. 15, pp. 3352–3355, 2006.

[22] X. Jia, G. Hu, F. Nitze et al., "Synthesis of palladium/helical carbon nanofiber hybrid nanostructures and their application for hydrogen peroxide and glucose detection," *ACS Applied Materials & Interfaces*, vol. 5, no. 22, pp. 12017–12022, 2013.

[23] H. Ma, L. Pan, Q. Zhao, and W. Peng, "Near-infrared response of a single carbon nanocoil," *Nanoscale*, vol. 5, no. 3, pp. 1153–1158, 2013.

[24] K. Akagi, R. Tamura, and M. Tsukada, "Electronic structure of helically coiled cage of graphitic carbon," *Physical Review Letters*, vol. 74, pp. 2307–2310, 1995.

[25] Q. Zhang, L. Yu, and Z. Cui, "Effects of the size of nano-copper catalysts and reaction temperature on the morphology of carbon fibers," *Materials Research Bulletin*, vol. 43, no. 3, pp. 735–742, 2008.

[26] E.-X. Ding, J. Wang, H.-Z. Geng et al., "Y-junction carbon nanocoils: Synthesis by chemical vapor deposition and formation mechanism," *Scientific Reports*, vol. 5, Article ID 11281, 2015.

[27] N. Tang, J. Wen, Y. Zhang, F. Liu, K. Lin, and Y. Du, "Helical carbon nanotubes: Catalytic particle size-dependent growth and magnetic properties," *ACS Nano*, vol. 4, no. 1, pp. 241–250, 2010.

[28] J. B. Bai, "Growth of nanotube/nanofibre coils by CVD on an alumina substrate," *Materials Letters*, vol. 57, no. 18, pp. 2629–2633, 2003.

[29] A. Shaikjee, P. J. Franklyn, and N. J. Coville, "The use of transmission electron microscopy tomography to correlate copper catalyst particle morphology with carbon fiber morphology," *Carbon*, vol. 49, no. 9, pp. 2950–2959, 2011.

[30] W. I. Hwang, H. Yanagida, and S. Motojima, "Vapor growth of carbon micro-coils by the Ni catalyzed pyrolysis of acetylene using rotating substrate," *Materials Letters*, vol. 43, no. 1, pp. 11–14, 2000.

[31] M. Kyotani, S. Matsushita, T. Nagai et al., "Helical carbon and graphitic films prepared from iodine-doped helical polyacetylene film using morphology-retaining carbonization," *Journal of the American Chemical Society*, vol. 130, no. 33, pp. 10880-10881, 2008.

[32] M. Goh, T. Matsushita, H. Satake, M. Kyotani, and K. Akagi, "Macroscopically aligned helical polyacetylene synthesized in magnetically oriented chiral nematic liquid crystal field," *Macromolecules* , vol. 43, no. 14, pp. 5943–5948, 2010.

[33] D. Fejes and K. Hernádi, "A review of the properties and CVD synthesis of coiled carbon nanotubes," *Materials* , vol. 3, no. 4, pp. 2618–2642, 2010.

[34] K.-D. Kim, S.-H. Kim, N. S. Kim, and D.-U. Kim, "Effect of the on/off cyclic modulation time ratio of C_2H_2/H_2 flow on the low temperature deposition of carbon nanofilaments," *Journal of Nanoscience and Nanotechnology*, vol. 7, no. 11, pp. 3969–3973, 2007.

[35] K.-D. Kim, S.-H. Kim, S. S. Yi, and K. Jang, "Effect of SF_6 incorporation in the cyclic process on the low temperature deposition of carbon nanofilaments," *Thin Solid Films*, vol. 518, no. 22, pp. 6412–6416, 2010.

[36] J. Eum, Y. Jeon, and S. Kim, "Effect of gas phase composition cycling on/off modulation numbers of C_2H_2/SF_6 flows on the formation of geometrically controlled carbon coils," *Journal of Nanoscience and Nanotechnology*, vol. 12, no. 7, pp. 6100–6106, 2012.

[37] Y.-C. Jeon, J.-H. Eum, S.-H. Kim, J.-C. Park, and S. I. Ahn, "Effect of the on/off cycling modulation time ratio of C_2H_2/SF_6 flows on the formation of geometrically controlled carbon coils," *Journal of Nanomaterials*, vol. 2012, Article ID 908961, 6 pages, 2012.

[38] Y.-C. Jeon, B. Park, S. Park, and S.-H. Kim, "Investigation of SF6 injection during cyclic C_2H_2/SF_6 flow for the formation of geometrically controlled carbon coils," *Journal of Nanoscience and Nanotechnology*, vol. 14, no. 12, pp. 9182–9188, 2014.

[39] G. H. Kang and S. H. Kim, "The formation of carbon microcoils having the coil-type overall geometry," *Journal of Coating Science and Technology*, vol. 2, pp. 100–104, 2015.

[40] G.-H. Kang, S.-H. Kim, and S. Park, "Controllable synthesis of carbon-nanocoil–carbon-microcoil hybrid materials," *Materials and Corrosion*, vol. 116, pp. 42–50, 2017.

[41] S. Park and S. Kim, "Controlled geometry formation of the carbon coils by the substrate pretreatment," *ISRN Nanomaterials*, vol. 2013, Article ID 893636, pp. 1–8, 2013.

[42] Y.-C. Jeon and S.-H. Kim, "Development of the geometry of carbon microcoils from carbon nanofilaments," *Vacuum*, vol. 107, pp. 219–224, 2014.

[43] S. Park, Y.-C. Jeon, and S.-H. Kim, "Effect of injection stage of SF6 flow on carbon micro coils formation," *ECS Journal of Solid State Science and Technology*, vol. 2, no. 11, pp. M56–M59, 2013.

[44] H. Bi, K. C. Kao, K. Ostrikov et al., "Unconventional Ni-P alloy-catalyzed CVD of carbon coil-like micro- and nano-structures," *Materials Chemistry and Physics*, vol. 116, no. 2-3, pp. 442–448, 2009.

[45] P. Scherrer, "Bestimmung der größe und der inneren struktur von kolloidteilchen mittels röntgenstrahlen, Nachrichten von der gesellschaft der wissenschaften zu göttingen," *Mathematisch-Physikalische Klasse*, vol. 1918, pp. 98–100, 1918.

[46] C.-T. Hsieh, Y.-T. Lin, J.-Y. Lin, and J.-L. Wei, "Synthesis of carbon nanotubes over Ni- and Co-supported $CaCO_3$ catalysts using catalytic chemical vapor deposition," *Materials Chemistry and Physics*, vol. 114, no. 2-3, pp. 702–708, 2009.

[47] X. Jian, Z. Zhou, S. Wu, L. Chen, Q. Zeng, and C. Wang, "Controllable preparation of Ni nanoparticles for catalysis of coiled carbon fibers growth," *Nanoscale Research Letters*, vol. 9, pp. 370–376, 2014.

[48] M. Sevilla and A. B. Fuertes, "Easy synthesis of graphitic carbon nanocoils from saccharides," *Materials Chemistry and Physics*, vol. 113, no. 1, pp. 208–214, 2009.

[49] K. C. Mondal, A. M. Strydom, R. M. Erasmus, J. M. Keartland, and N. J. Coville, "Physical properties of CVD boron-doped multiwalled carbon nanotubes," *Materials Chemistry and Physics*, vol. 111, no. 2-3, pp. 386–390, 2008.

[50] S. Yang, X. Chen, T. Katsuno, and S. Motojima, "Controllable synthesis of carbon microcoils/nanocoils by catalysts supported on ceramics using catalyzed chemical vapor deposition process," *Materials Research Bulletin*, vol. 42, no. 3, pp. 465–473, 2007.

[51] J. Robertson, "Diamond-like amorphous carbon," *Materials Science and Engineering: R: Reports*, vol. 37, pp. 129–282, 2002.

[52] E. P. Sajitha, V. Prasad, S. V. Subramanyam, S. Eto, K. Takai, and T. Enoki, "Synthesis and characteristics of iron nanoparticles in a carbon matrix along with the catalytic graphitization of amorphous carbon," *Carbon*, vol. 42, no. 14, pp. 2815–2820, 2004.